

# PHYSICAL REVIEW LETTERS

---

---

VOLUME 78

10 FEBRUARY 1997

NUMBER 6

---

---

## Bose-Einstein Condensation of Lithium: Observation of Limited Condensate Number

C. C. Bradley, C. A. Sackett, and R. G. Hulet

*Physics Department and Rice Quantum Institute, Rice University, Houston, Texas 77005-1892*

(Received 5 September 1996; revised manuscript received 23 October 1996)

Bose-Einstein condensation of  ${}^7\text{Li}$  has been studied in a magnetically trapped gas. Because of the effectively attractive interactions between  ${}^7\text{Li}$  atoms, many-body quantum theory predicts that the occupation number of the condensate is limited to about 1400 atoms. We observe the condensate number to be limited to a maximum value between 650 and 1300 atoms. The measurements were made using a versatile phase-contrast imaging technique. [S0031-9007(97)02369-7]

PACS numbers: 03.75.Fi, 05.30.Jp, 32.80.Pj

In a previous Letter [1] we reported evidence for Bose-Einstein condensation (BEC) in a magnetically trapped atomic gas of  ${}^7\text{Li}$ . Unlike  ${}^{87}\text{Rb}$  and  ${}^{23}\text{Na}$ , the other species in which gaseous BEC has been observed [2],  ${}^7\text{Li}$  atoms have a negative  $s$ -wave scattering length  $a$ , indicating that for a sufficiently cold and dilute gas the interatomic interactions are effectively attractive. Attractive interactions are thought to prevent BEC from occurring at all in a spatially homogeneous (i.e., untrapped) gas [3,4], and as recently as 1994, these interactions were believed to preclude BEC in a trap as well. Current theories predict that BEC can occur in a trap such as ours, but with no more than about 1400 condensate atoms [5–11]. Verification of this prediction would provide a sensitive test of many-body quantum theory. In our previous work [1], the condensate could not be directly observed, and the number of condensate atoms suggested by the measurements was overestimated. In this Letter we report quantitative measurements of the condensate number, which are consistent with the theoretical limit.

The effects of interactions on a trapped condensate are studied using mean-field theory. For densities  $n$  such that  $na^3 \ll 1$ , the mean-field interaction energy is given by  $U = 4\pi\hbar^2 an/m$ , where  $m$  is the atomic mass. For  ${}^7\text{Li}$ ,  $a = (-14.5 \pm 0.4) \text{ \AA}$  [12]. Because  $a < 0$ , the interaction energy decreases with increasing  $n$ , so the condensate tends to collapse upon itself. When the confining potential is included in the theory, it is found that if  $U$  is sufficiently small compared to the trap energy-level spacing, the destabilizing influence of

the interactions is balanced by the kinetic pressure of the gas, and a metastable condensate can form. This requirement for  $U$  leads to the prediction that the number of condensate atoms  $N_0$  is limited. As the maximum  $N_0$  is approached, the rate for inelastic collisions increases and the gas becomes progressively less stable with respect to thermal and quantum mechanical fluctuations [7–10].

The apparatus used to produce BEC has been described in previous publications [1,13]. The magnetic trap forms a nearly symmetric harmonic oscillator potential, with oscillation frequencies  $\nu_x = 150.6 \text{ Hz}$ ,  $\nu_y = 152.6 \text{ Hz}$ , and  $\nu_z = 131.5 \text{ Hz}$ . The bias field at the center of the trap is 1003 G [14]. The trap is loaded using laser cooling, resulting in a number of trapped atoms  $N \approx 2 \times 10^8$ , and a temperature  $T \approx 200 \mu\text{K}$ . The atoms are then cooled into the quantum degenerate regime using rf-induced forced evaporative cooling [15]. Quantum degeneracy is reached with  $N \approx 10^5$  atoms at  $T \approx 300 \text{ nK}$ , after  $\sim 200$  sec of cooling.

After cooling, the trapped atom distribution is observed by imaging via an optical probe. This technique has previously been used to measure the spatial density distribution directly [16] and to measure the velocity distribution by first releasing the atoms from the trap and allowing them to ballistically expand [2]. In our experiment, the trap is formed by permanent magnets, so only *in situ* imaging is possible. The harmonic oscillator ground state of our trap has a Gaussian density distribution with a  $1/e$  radius of  $3 \mu\text{m}$ . The resolution of the imaging system must therefore be sufficient to detect

such a small object. In our previous experiment [1] the imaging resolution was not sufficient, but the presence of the spatially localized condensate was deduced from distortions observed in images of quantum degenerate clouds [17].

Our improved imaging system is shown schematically in Fig. 1. With the polarizer E removed, it can be used to measure the density distribution by absorption imaging, in which the absorptive shadow of the atoms is imaged onto the camera. However, any imaging system with finite resolution will be sensitive to phase shifts caused by the index of refraction of the atom cloud, which can result in significant image distortions. In order to eliminate these distortions, it is necessary to reduce the index by using large probe detunings  $\Delta$ . Since the absorption coefficient decreases as  $\Delta^{-2}$ , while the index decreases as only  $\Delta^{-1}$ , eliminating the distortions can leave the absorption signal too small to be detected.

Phase-contrast techniques are commonly employed to image weakly absorbing objects [18]. In passing through the cloud, the laser acquires a spatially dependent phase  $\beta = \phi + i\alpha/2$ , where  $\phi$  is the dispersive phase shift and  $\alpha$  is the optical density. The probe electric field  $\mathbf{E}$  can then be written as  $\mathbf{E} = \mathbf{E}_o e^{i\beta}$ . In absorption imaging, the detected signal intensity  $I_s$  depends only on  $\alpha$ :  $I_s = I_o |e^{i\beta}|^2 = I_o e^{-\alpha}$ , where  $I_o = |\mathbf{E}_o|^2$ . In the simplest phase-contrast technique, dark-field imaging, a spatially small opaque beam block is inserted at a focus of the probe laser beam (position D in Fig. 1). The resulting signal is  $I_s = I_o |e^{i\beta} - 1|^2 \approx I_o \phi^2$  for  $\alpha \ll |\phi| \ll 1$ . Andrews *et al.* used this technique to image  $^{23}\text{Na}$  Bose-Einstein condensates *in situ* [16]. However, minimizing refractive distortions requires  $|\phi| \ll 1$ , so the dark-field signal is relatively small as it is proportional to  $\phi^2$ . Because the number of condensate atoms in  $^7\text{Li}$  is limited, a more sensitive technique is required.

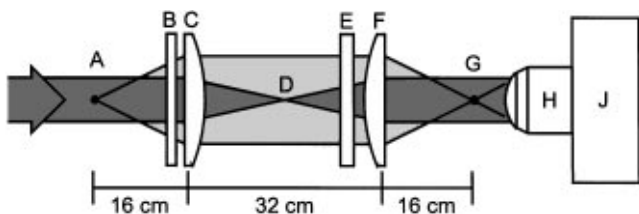


FIG. 1. A schematic of the imaging system used for *in situ* phase-contrast polarization imaging. A linearly polarized laser beam is directed through the cloud of trapped atoms located at A. The probe beam and scattered light field pass out of a vacuum viewport B, and are relayed to the primary image plane G by an identical pair of 3-cm diameter, 16-cm focal-length doublet lenses C and F. The light is then reimaged and magnified onto a camera J by a microscope objective H. The measured magnification is 19, and the camera pixels are  $19 \mu\text{m}$  square. The linear polarizer E causes the scattered light and probe fields to interfere, producing an image sensitive to the refractive index of the cloud. The system is focused by adjusting the position of lens F, which is mounted on a translator.

We use a flexible phase-contrast method which exploits the birefringence of the atoms in a strong magnetic field. The probe beam is linearly polarized perpendicular to the magnetic field axis and propagates along an axis inclined  $55^\circ$  with respect to the field. The electric field of the probe decomposes into two elliptical polarizations  $\mathbf{E} = \mathbf{E}_c + \mathbf{E}_{nc}$ , such that  $\mathbf{E}_c$  couples to the  $\sigma^+$  optical transition and acquires a phase shift, while  $\mathbf{E}_{nc}$  does not. If the transmitted light is passed through a polarizer (E in Fig. 1),  $\mathbf{E}_c$  and  $\mathbf{E}_{nc}$  combine and interfere, producing a phase-contrast image. If  $\Delta$  is large enough that  $\alpha$  can be neglected, the detected intensity distribution is

$$I_s(r) = I_o \left[ \cos^2 \theta + \frac{\sqrt{3}}{4} \phi(r) \sin 2\theta - \frac{3}{16} \phi(r)^2 \cos 2\theta \right], \quad (1)$$

where  $\theta$  is the angle between the polarizer axis and the initial polarization of the probe beam. Linear phase-contrast imaging is accomplished for  $\theta = 45^\circ$  and dark-field imaging is recovered for  $\theta = 90^\circ$ . By varying  $\theta$  between these extremes, the relative size of the signal and background can be varied in order to maximize the signal-to-noise ratio of the image. For the data reported here,  $\theta = \pm 75^\circ$ .

The cloud is probed by a pulsed laser beam with a duration of  $10 \mu\text{s}$ , an intensity of  $250 \text{ mW}/\text{cm}^2$  and with  $\Delta$  in the range  $20\Gamma < |\Delta| < 40\Gamma$ , where  $\Gamma = 5.9 \text{ MHz}$  is the natural linewidth of the transition. Only one image can be obtained because each atom scatters a few photons while being probed, heating the gas to several  $\mu\text{K}$ .

The detected signal intensity, given by Eq. (1), is related to the density distribution  $n$  of the trapped atoms by [19]

$$\beta(x', y') = \phi + i \frac{\alpha}{2} = -\frac{\sigma_0}{2} \int dz' n(x', y', z') \frac{\Gamma}{2\Delta + i\Gamma}, \quad (2)$$

where  $\sigma_0 = 1.43 \times 10^{-9} \text{ cm}^2$  is the resonant light scattering cross section. The  $z'$  axis is parallel to the probe propagation axis, while the  $x'$  and  $y'$  axes are perpendicular to it. Light scattering might be modified by the quantum degenerate nature of the atoms, but this effect is expected to be negligible under our conditions [20].

Because the trap is not isotropic, the density distributions are slightly ellipsoidal; the images are observed to have the expected asymmetry. The radial profiles shown in Fig. 2 are obtained by angle averaging the data around ellipses with aspect ratio 1.10, accounting for the trap asymmetry and the oblique viewing angle [21]. We assume that the gas is in thermal equilibrium, and fit  $T$  and  $N_0$  to the data. Any two of  $N$ ,  $T$ , or  $N_0$  completely determine the density of the gas through the Bose-Einstein distribution function. The density is calculated using a semiclassical ideal-gas approximation for the noncondensed atoms [22],

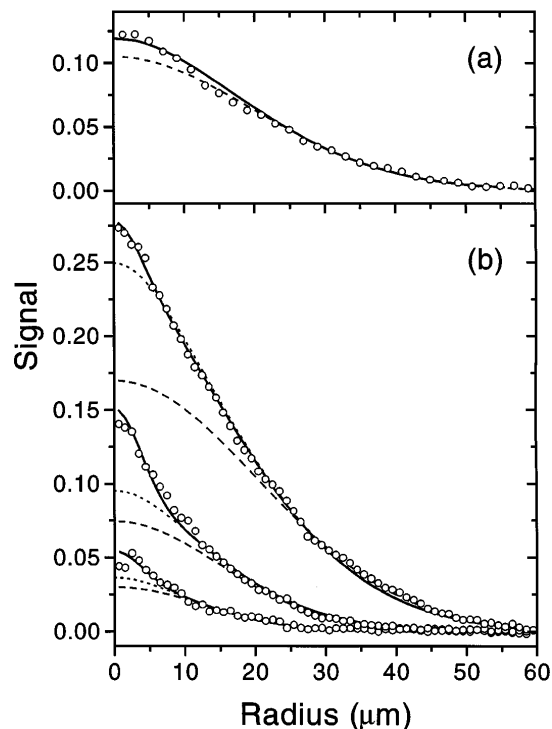


FIG. 2. Spatial profiles of trapped ultracold  ${}^7\text{Li}$  gas. The vertical axis gives the magnitude of the phase-contrast signal intensity relative to the probe intensity. The data points are taken from observed images. The solid curves are calculated by fitting Bose-Einstein distributions to the data, the short-dashed curves are the same distributions with the condensate atoms removed, and the long-dashed curves are classical (Gaussian) distributions fit to the tails of the data. The calculated signals are convolved with a Gaussian function to account for the limited resolution of the imaging system, assuming an effective resolution of  $4\ \mu\text{m}$ . For the data in (a), the probe detuning was  $+191\ \text{MHz}$ , and the fitted distribution has  $9.0 \times 10^4$  atoms at a temperature of  $309\ \text{nK}$ . The number of condensate atoms is  $\sim 1$ , indicating that the gas is just approaching degeneracy. In (b) a sequence of profiles that exhibits condensate peaks is shown. From the strongest to weakest signals, the total number of atoms and fitted temperatures are  $1.01 \times 10^5$  atoms at  $304\ \text{nK}$ ;  $2.6 \times 10^4$  atoms at  $193\ \text{nK}$ ; and  $6.6 \times 10^3$  atoms at  $122\ \text{nK}$ . The corresponding numbers of condensate atoms are 500, 810, and 270, respectively. The probe detuning for these data was  $-130\ \text{MHz}$ .

and a Gaussian function for the condensate. The solid lines in Fig. 2 show the results of the fits.

For temperatures sufficiently greater than the critical temperature  $T_c$ , the gas can be described by the Boltzmann distribution, which predicts a Gaussian density profile. The long-dashed lines in Fig. 2 are Gaussian functions fit to the tails of the distributions, which approximate the data only in Fig. 2(a). Figure 2(b) shows three distributions for which  $T < T_c$ . For these distributions, the density is distinctly non-Gaussian, due to an enhanced central peak. Comparison between Fig. 2(a) and the upper curve in Fig. 2(b) is striking, as these distributions correspond to nearly the same temperature, but differ by about 10% in number. The short-dashed curves in Fig. 2(b) show the calculated distributions with the

condensate contribution subtracted. As comparison of the short-dashed and solid curves indicates, the increase in peak signal is caused by both condensed and noncondensed atoms. The contribution of the noncondensed atoms is significant for the upper curve, but at lower temperatures, the contribution of the condensate makes up most of the enhanced peak.

Analysis of the data is complicated by the fact that the condensate size is on the order of the imaging resolution. The resolution can be included in the fit by convolving the theoretical signal with the point transfer function (PTF) of the imaging system [23]. The PTF is calculated by analyzing the propagation of light through the system, given the known lens geometry. In order to test this calculation, we used the system to image laser light emerging from an optical fiber. The intensity distribution of the light in the fiber is Gaussian with a  $1/e$  radius of  $1.2\ \mu\text{m}$ , so that it approximates a point source. Fig. 3 shows cross sections of the images obtained with the system focused at two different points. The narrower peak shown has a  $1/e$  radius of  $3.0\ \mu\text{m}$ , as compared with  $2.5\ \mu\text{m}$  expected for a diffraction-limited lens (dotted line). The curves are the results of convolving the fiber source with the calculated PTF.

Since the images of the atom cloud are produced by coherently diffracted light, the PTF convolution is performed on the electric field. The results of the coherent field convolution indicate that the primary effect of the coherence is to reduce the importance of the tail of the PTF, because the phase of the field in the tail is rapidly varying. In addition, the PTF depends on where the imaging system is focused, as Fig. 3 shows. When imaging the atom cloud, the focal position can be determined to  $\pm 200\ \mu\text{m}$  by observing image distortions which occur when the system is further off focus. Given this uncertainty, and the unimportance of the tail, the PTF convolution is well approximated by an incoherent convolution of the image intensity with a Gaussian function of appropriate  $1/e$  radius  $R$ . The experimental range of focal positions corresponds to values of  $R$  ranging from  $2.5$  to  $5\ \mu\text{m}$ . This uncertainty in the effective resolution is the dominant source of error in our determination of  $N_0$ .

We have observed degenerate conditions for  $T$  between  $120$  and  $330\ \text{nK}$ , and for  $N$  between  $6800$  and  $135\ 000$  atoms. In all cases,  $N_0$  is found to be relatively small. Fitting with  $R = 5\ \mu\text{m}$ , the maximum  $N_0$  observed is about  $1300$  atoms. This value drops to  $1000$  for  $R = 4\ \mu\text{m}$ , and to  $650$  for  $R = 2.5\ \mu\text{m}$ . No systematic effects were observed as either the sign or magnitude of the detuning or the polarizer angle were varied, confirming the relations given in Eqs. (1) and (2).

In the analysis, we have assumed that the gas is ideal, but interactions are expected to alter the size and shape of the density distribution. Mean-field theory predicts that interactions will reduce the  $1/e$  radius of the condensate from  $3\ \mu\text{m}$  for low occupation number

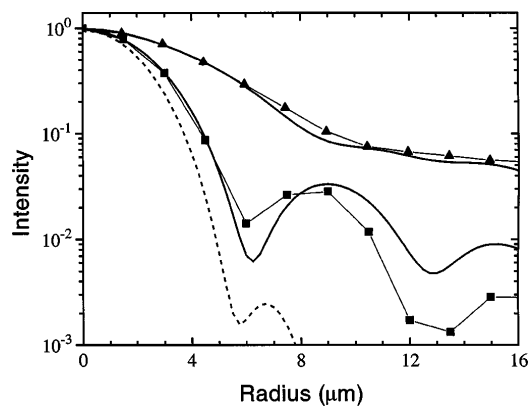


FIG. 3. Test images of an optical fiber. The data points are obtained from cross sections through images of the light emitted by an optical fiber. The squares indicate data obtained with the imaging system at its best focus, while the triangles indicate data obtained with the system defocused by  $200 \mu\text{m}$ . The solid curves are the expected intensity patterns, while the dashed curve is the expected pattern for a well-focused system in the absence of lens aberrations. The curves are obtained by calculating the PTF of the system as the Fourier transform of the system aperture function and the phase error due to the lenses [23]. The PTF is convolved with a Gaussian electric field with  $1.75 \mu\text{m}$   $1/e$  radius to account for the size of the optical fiber mode, and squared to obtain the intensity. The resulting pattern is then averaged to reflect the pixel size of the camera. The phase errors are due to spherical aberration of  $0.5 \lambda/\text{cm}^4$ , as calculated by ray tracing.

to  $\sim 2 \mu\text{m}$  as the maximum  $N_0$  is approached [6,8–11]. If the smaller condensate radius is used in the fit, the maximum values for  $N_0$  decrease, becoming  $\sim 1050$  for  $R = 5 \mu\text{m}$ . The size of the condensate is not expected to change appreciably for  $N_0 < 1000$ , so the values obtained for  $R = 2.5$  and  $4 \mu\text{m}$  are not sensitive to interactions. Interactions are not expected to significantly affect the distribution of the noncondensed atoms [10,24], because at the critical density the mean interaction energy of  $\sim 1$  nK is much smaller than  $T$ .

An estimate of our sensitivity to condensate atoms can be obtained from the fitting procedure. By fixing  $N_0$  and fitting  $T$  to the data,  $\chi^2$  can be determined as a function of  $N_0$ . Since  $N_0$  mostly affects the central part of the distribution, we define a restricted, unnormalized  $\chi^2$  by summing over the squares of the differences between the calculated distributions and the data for radii less than  $10 \mu\text{m}$ . Calculating  $\chi^2(N_0)$  for several images with large values of  $N_0$  indicates that  $\chi^2$  is increased by a factor of 2 from its minimum value when  $N_0$  is varied by about 150 atoms, roughly independent of  $R$ .

The sensitivity of  $N_0$  to  $R$  could be reduced by observing a distribution consisting mainly of condensate atoms. Since the integrated intensity of an image is independent of lens aberrations,  $N_0$  could be determined simply by measuring the number of atoms in the trap. It may be possible to produce such a distribution through a final accelerated stage of evaporative cooling once BEC has occurred, but

we have not yet successfully done so. Systematic studies of the process are technically difficult because fluctuations of the trap bias field must be less than  $\sim 50 \mu\text{G}$  to allow repeated production of pure condensates.

In summary, we have observed BEC in a gas with attractive interactions, by obtaining *in situ* images of degenerate clouds of atoms. The number of condensate atoms is found to be limited to a value consistent with recent theoretical predictions. The range of numbers and temperatures across which the limit is observed to hold suggests that the limit is fundamental, rather than technical. Future experiments are anticipated that will investigate the dynamics of the formation, decay, and collapse of the condensates [7–11].

We are grateful for helpful discussions with T. Bergeman, W. Ketterle, H. Stoof, E. Timmermans, N. Vansteenkiste, M. Welling, and C. Westbrook. This work is supported by the National Science Foundation and the Welch Foundation.

- [1] C. C. Bradley, C. A. Sackett, J. J. Tollett, and R. G. Hulet, *Phys. Rev. Lett.* **75**, 1687 (1995).
- [2] M. H. Anderson *et al.*, *Science* **269**, 198 (1995); K. B. Davis *et al.*, *Phys. Rev. Lett.* **75**, 3969 (1995); M.-O. Mewes *et al.*, *Phys. Rev. Lett.* **77**, 416 (1996).
- [3] L. D. Landau and E. M. Lifshitz, *Statistical Physics* (Pergamon, London, 1958), 1st ed.
- [4] H. T. C. Stoof, *Phys. Rev. A* **49**, 3824 (1994).
- [5] P. A. Ruprecht, M. J. Holland, K. Burnett, and M. Edwards, *Phys. Rev. A* **51**, 4704 (1995).
- [6] F. Dalfovo and S. Stringari, *Phys. Rev. A* **53**, 2477 (1996).
- [7] Y. Kagan, G. V. Shlyapnikov, and J. T. M. Walraven, *Phys. Rev. Lett.* **76**, 2670 (1996).
- [8] R. J. Dodd *et al.*, *Phys. Rev. A* **54**, 661 (1996).
- [9] H. T. C. Stoof, LANL Report No. cond-mat/9601150 (to be published).
- [10] M. Houbiers and H. T. C. Stoof, *Phys. Rev. A* **54**, 5055 (1996).
- [11] T. Bergeman (to be published).
- [12] E. R. I. Abraham, W. I. McAlexander, C. A. Sackett, and R. G. Hulet, *Phys. Rev. Lett.* **74**, 1315 (1995).
- [13] J. J. Tollett, C. C. Bradley, C. A. Sackett, and R. G. Hulet, *Phys. Rev. A* **51**, R22 (1995).
- [14] The trap frequencies and bias field differ from those reported in Ref. [1] because the magnets have been replaced.
- [15] See W. Ketterle and N. J. van Druten, in *Advances in Atomic, Molecular, and Optical Physics*, edited by B. Bederson and H. Walther (Academic Press, San Diego, 1996), No. 37, p. 181, and references therein.
- [16] M. R. Andrews *et al.*, *Science* **273**, 84 (1996).
- [17] It was suggested in Ref. [1] that the distortions were caused by the scattering of probe light by the condensate, in conjunction with diffraction by the lens aperture. Subsequent analysis has shown that lens aberrations were more important than the aperture, but confirms that the distortions did indicate the presence of a condensate. This analysis will be described in a separate publication.
- [18] See, for instance, E. Hecht, *Optics* (Addison-Wesley, Reading, Massachusetts, 1987), 2nd ed.

- 
- [19] See, for instance, P. Meystre and M. Sargent III, *Elements of Quantum Optics* (Springer-Verlag, Berlin, 1991), 2nd ed.
- [20] O. Morice, Y. Castin, and J. Dalibard, *Phys. Rev. A* **51**, 3896 (1995).
- [21] The condensate itself is expected to have an aspect ratio of 1.05, but this difference is not discernible with our imaging resolution.
- [22] V. Bagnato, D.E. Pritchard, and D. Kleppner, *Phys. Rev. A* **35**, 4354 (1987). The semiclassical distribution was compared to an exact calculation and found to be accurate, except for a temperature shift as noted in W. Ketterle and N.J. van Druten, *Phys. Rev. A* **54**, 656 (1996). All the temperatures reported here are calculated in the semiclassical approximation.
- [23] See, for instance, M. Born and E. Wolf, *Principles of Optics* (Pergamon Press, New York, 1959).
- [24] T. Bergeman (private communication).